

Level-Set Minimization of Potential Controlled Hadwiger Valuations for Molecular Solvation

Li-Tien Cheng* Bo Li[†] Zhongming Wang[‡]

January 21, 2010

Abstract

A level-set method is developed for the numerical minimization of a class of Hadwiger valuations with a potential on a set of three-dimensional bodies. Such valuations are linear combinations of the volume, surface area, and surface integral of mean curvature. The potential increases rapidly as the body shrinks beyond a critical size. The combination of the Hadwiger valuation and the potential is the mean-field free-energy functional of the solvation of non-polar molecules in the recently developed variational implicit-solvent model. This functional of surfaces is minimized by the level-set evolution in the steepest descent of the free energy. The normal velocity of this surface evolution consists of both the mean and Gaussian curvatures, and a lower-order, “forcing” term arising from the potential. The forward Euler method is used to discretize the time derivative with a dynamic time stepping that satisfies a CFL condition. The normal velocity is decomposed into two parts. The first part consists of both the mean and Gaussian curvature terms. It is of parabolic type with parameter correction, and is discretized by central differencing. The second part has all the lower-order terms. It is of hyperbolic type, and is discretized by an upwinding scheme. New techniques of local level-set method and numerical integration are developed. Numerical tests demonstrate a second-order convergence of the method. Examples of application to the modeling of molecular solvation are presented.

Keywords: the level-set method, Hadwiger valuations, the Lennard-Jones potential, normal velocity, mean curvature, Gaussian curvature, molecular solvation.

*Department of Mathematics, University of California, San Diego, 9500 Gilman Drive, Mail code: 0112, La Jolla, CA 92093-0112, USA. Email: lcheng@math.ucsd.edu.

[†]Department of Mathematics and Center for Theoretical Biological Physics, University of California, San Diego, 9500 Gilman Drive, Mail code: 0112, La Jolla, CA 92093-0112, USA. Email: bli@math.ucsd.edu.

[‡]Department of Chemistry and Biochemistry, Department of Mathematics, and Center for Theoretical Biological Physics, University of California, San Diego, 9500 Gilman Drive, Mail code: 0112, La Jolla, CA 92093-0112, USA. E-mail: z2wang@math.ucsd.edu.

1 Introduction

The classical Hadwiger’s Theorem in differential geometry states that a valuation (i.e., a functional) defined on certain class of three-dimensional bodies satisfying some conditions similar to those of a measure must be a linear combination of the volume, surface area, surface integral of mean curvature, and surface integral of Gaussian curvature [10, 11]. The combination of such a valuation and a potential is the recently proposed free-energy functional for the solvation of non-polar molecules in aqueous solution [7, 8]. More precisely, this free energy $G[\Gamma]$ is defined for all possible surfaces Γ that enclose a given set of points $\mathbf{x}_1, \dots, \mathbf{x}_N$, and is given by

$$G[\Gamma] = P\text{Vol}(\Omega_{in}) + \gamma_0\text{Area}(\Gamma) - 2\gamma_0\tau \int_{\Gamma} H dS + \rho_0 \int_{\Omega_{ex}} U(\mathbf{x})dV. \quad (1.1)$$

Here, Ω_{in} and Ω_{ex} are the interior (bounded) region and the exterior (unbounded) region of the space \mathbb{R}^3 , respectively, separated by the closed surface Γ , cf. Figure 1 in which \mathbf{n} denotes the unit normal at the interface Γ pointing from Ω_{in} to Ω_{ex} . All the points \mathbf{x}_i ($i = 1, \dots, N$) are inside Ω_{in} . All P , γ_0 , τ , and ρ_0 are positive constants, H is the mean curvature, and U is a given function defined on $\mathbb{R}^3 \setminus \{\mathbf{x}_1, \dots, \mathbf{x}_N\}$.

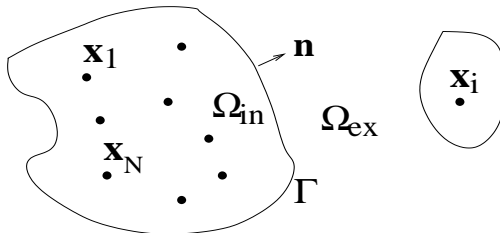


Figure 1: A schematic description of the geometry related to the functional (1.1).

In modeling the solvation of molecules, the regions Ω_{in} and Ω_{ex} represent those of solute molecule and solvent, respectively. The region Ω_{in} can have multiple components. The fixed points $\mathbf{x}_1, \dots, \mathbf{x}_N$ are centers of solute atoms. The first term in (1.1) describes the work needed to create the solute region Ω_{in} in the solvent against the pressure difference P between the liquid and vapor phases. The second and third terms in (1.1) describe the surface energy cost due to restructuring of molecules near the interface Γ . In these terms, γ_0 is the usual surface tension for a planar surface, and the integral of H is the surface energy correction with τ a correction parameter, often called the Tolman length. Such a correction is needed for interfacial systems at the molecular scale. The last term in (1.1) describes the solute-solvent interaction through a potential function U . Here the solvent is treated as a continuum with a uniform solvent density ρ_0 . The potential U is given by

$$U(\mathbf{x}) = \sum_{i=1}^N U_{LJ}^{(i)}(|\mathbf{x} - \mathbf{x}_i|) \quad \forall \mathbf{x} \in \mathbb{R}^3 \setminus \{\mathbf{x}_1, \dots, \mathbf{x}_N\}. \quad (1.2)$$

Each $U_{LJ}^{(i)}$ is a Lennard-Jones potential (cf. Figure 2)

$$U_{LJ}^{(i)}(r) = 4\epsilon_i \left[\left(\frac{\sigma_i}{r} \right)^{12} - \left(\frac{\sigma_i}{r} \right)^6 \right], \quad (1.3)$$

where $\epsilon_i > 0$ and $\sigma_i > 0$ are given parameters for all $i = 1, \dots, N$.

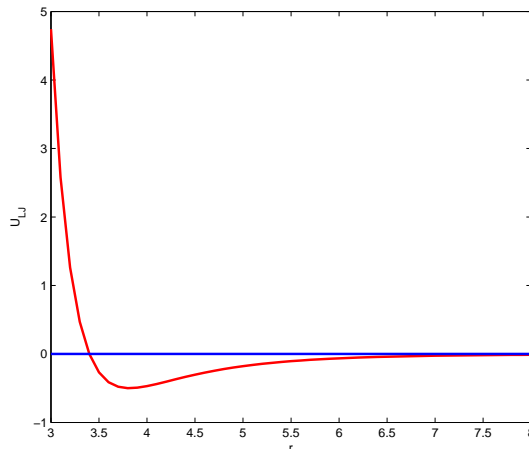


Figure 2: The Lennard-Jones potential.

Note that the free-energy functional (1.1) does not have the surface integral of the Gaussian curvature, a term that is included in a general Hadwiger valuation. By the Gauss–Bonnet Theorem, this integral is $2\pi\chi(\Gamma)$, where $\chi(\Gamma)$ is the Euler characteristic of Γ . The integral remains as a constant as long as no topological changes of the surface Γ occurs. Even if the surface Γ undergoes a topological change, the contribution from the surface integral of the Gaussian curvature is only an additive constant. It will not affect the minimization of the functional. In fact it is easy to see that, with respect to the Hausdorff distance of sets, a surface of m components (with $m \geq 1$ an integer) is a local minimizer of the functional (1.1), if and only if it is a local minimizer of the functional which consists of all the terms in $G[\Gamma]$ in (1.1) and the integral of the Gaussian curvature, among all the m -component surfaces.

In this work, we develop an efficient and accurate (local) level-set method to minimize the functional (1.1) to determine the free-energy minimizing interface Γ_{min} and the corresponding minimum free energy $G[\Gamma_{min}]$. In this method, an initial surface is evolved in the direction of the steepest descent to a (local) minimum of the free-energy functional. The surface evolution is determined and tracked by solving the level-set equation for a level-set function whose zero level set gives the evolving surface. The normal velocity that defines the level-set equation is given by the the minus first variation of the free-energy functional (1.1) with respect to the location change of the surface Γ .

To be more precise, let us denote the evolving surface by $\Gamma = \Gamma(t)$ at time t . This surface can be represented as the zero level set of a level-set function $\phi = \phi(\mathbf{x}, t)$ with $\mathbf{x} \in \mathbb{R}^3$, i.e.,

$$\Gamma(t) = \{\mathbf{x} \in \mathbb{R}^3 : \phi(\mathbf{x}, t) = 0\}.$$

The level-set function $\phi = \phi(\mathbf{x}, t)$ is the solution of the level-set equation [12, 13, 17]

$$\phi_t + v_n |\nabla \phi| = 0, \quad (1.4)$$

where v_n is the normal velocity that determines the motion of the evolving surface. It is defined at any point $\mathbf{x} = \mathbf{x}(t) \in \Gamma = \Gamma(t)$ by $v_n(\mathbf{x}, t) = (d\mathbf{x}(t)/dt) \cdot \mathbf{n}(\mathbf{x})$, where $\mathbf{n}(\mathbf{x})$ is the unit normal of the surface $\Gamma(t)$ at the point \mathbf{x} pointing from Ω_{in} to Ω_{ex} (cf. Figure 1).

We evolve the surface in the direction of steepest descent of the free energy. This means that we choose the normal velocity to be

$$v_n = -\delta_\Gamma G[\Gamma],$$

where δ_Γ denotes the variation with respect to the location change of the surface Γ along its normal direction. Therefore, at any point \mathbf{x} on the surface Γ , the normal velocity is [14, 15]

$$v_n(\mathbf{x}) = -P - 2\gamma_0[H(\mathbf{x}) - \tau K(\mathbf{x})] + \rho_0 U(\mathbf{x}), \quad (1.5)$$

where $H(\mathbf{x})$ and $K(\mathbf{x})$ are the mean and Gaussian curvatures of the surface Γ at the point \mathbf{x} . As usual, we extend the normal velocity v_n from the surface Γ onto a three-dimensional region surrounding Γ so that the level-set equation (1.4) can be solved. This region can be the entire computational box or a narrow band around the surface Γ . With such a normal velocity, we have formally that

$$\frac{d}{dt} G[\Gamma(t)] = \int_{\Gamma(t)} \delta_\Gamma G[\Gamma(t)] \left[\frac{d\mathbf{x}(t)}{dt} \cdot \mathbf{n} \right] dS = - \int_{\Gamma(t)} [v_n(\mathbf{x})] dS \leq 0.$$

This confirms that the free energy decays during the surface evolution by the defined normal velocity.

We analyze the level-set equation to find out the condition under which the level-set equation is a (degenerated) parabolic equation. Based on such an analysis, we decompose the part $-v_n |\nabla \phi|$ in the level-set equation (1.4) into a parabolic part (after a parameter correction) and hyperbolic part. We treat the parabolic part using the central difference scheme and treat the hyperbolic part using an upwinding scheme. In addition to classical level-set techniques, such as the local level-set method and reinitialization of the level-set function [12, 17], we also develop a technique of accurate, fast, and stable numerical integration of a Lennard-Jones type function. This technique is particularly useful to treat the possible numerical instability due to the dramatic change of the Lennard-Jones potential $U_{LJ}(r)$ near $r = 0$. Our numerical tests show that our method is of second-order convergence. We finally apply our methods to the solvation of some molecular systems.

We remark that we initiated our method before and applied a preliminary version of the method to the level-set simulation of non-polar molecular systems, cf. [3, 5, 6, 18]. Our method has now been much refined. The current work is the first that is focused on the mathematical and numerical aspects and that gives the details of the method.

Section 2 below presents an analysis and discretization of the level-set equation (1.4). Section 3 gives our numerical algorithm with some computational details. Section 4 describes

in details a technique of numerical integration in our level-set method. Section 5 is the convergence test. Section 6 shows examples of applications of our method to some molecular systems. Finally, Section 7 presents conclusions. Appendix has proofs of some identities related to the curvatures and their linearizations.

2 Discretization

We first consider the spatial discretization of the level-set equation (1.4). We rewrite this equation as

$$\phi_t = -v_n |\nabla \phi| = A + B |\nabla \phi|, \quad (2.1)$$

where A and B are defined by (dropping the time dependence)

$$A(\mathbf{x}) = 2\gamma_0 [H(\mathbf{x}) - \tau K(\mathbf{x})] |\nabla \phi(\mathbf{x})| \quad \text{and} \quad B(\mathbf{x}) = P - \rho_0 U(\mathbf{x}), \quad (2.2)$$

respectively. If there were only the second part (the B part), i.e., the equation were $\phi_t = B |\nabla \phi|$, then this would be a hyperbolic type equation. We therefore discretize the term $B |\nabla \phi|$ using an upwinding scheme. In our implementation, we use a fifth-order WENO (weighted essential-no-oscillation) scheme.

To discretize the A part in (2.2), we need to analyze the mean and Gaussian curvatures. Fix a point \mathbf{x} , not necessary on the surface Γ . Denote by $\kappa_1 = \kappa_1(\mathbf{x})$ and $\kappa_2 = \kappa_2(\mathbf{x})$ the two principal curvatures of the level surface of the function ϕ at \mathbf{x} . If $\nabla \phi$ is nonzero at this point, then the mean curvature and Gaussian curvature of this level surface at \mathbf{x} are given by [12, 17]

$$H = \frac{1}{2}(\kappa_1 + \kappa_2) = \frac{1}{2} \nabla \cdot \left(\frac{\nabla \phi}{|\nabla \phi|} \right), \quad (2.3)$$

$$K = \kappa_1 \kappa_2 = \frac{\nabla \phi}{|\nabla \phi|} \cdot \text{adj}(\nabla^2 \phi) \frac{\nabla \phi}{|\nabla \phi|}, \quad (2.4)$$

respectively, where $\text{adj}(\nabla^2 \phi)$ is the adjoint matrix of the Hessian matrix $\nabla^2 \phi = (\partial_{x_i x_j}^2 \phi)$ of the level-set function ϕ (assuming all the second-order derivatives of ϕ exist).

Define now the 3×3 matrices $P = P(\mathbf{x})$ and $\Pi = \Pi(\mathbf{x})$, respectively, by [1, 9, 12, 17]

$$P = I - \frac{\nabla \phi \otimes \nabla \phi}{|\nabla \phi|^2}, \quad (2.5)$$

$$\Pi = \frac{1}{|\nabla \phi|} P (\nabla^2 \phi) P. \quad (2.6)$$

Both P and Π are symmetric matrices. The matrix $P = P(\mathbf{x})$ is the matrix of projection onto the tangent plane of the level surface of ϕ at \mathbf{x} . It has three eigenvalues 0, 1, and 1 with 0 corresponding to any eigenvector parallel to the normal $\nabla \phi(\mathbf{x})$ and 1 corresponding to eigenvectors tangent to the level surface. The projection of the matrix $\Pi = \Pi(\mathbf{x})$ onto this tangent plane is exactly the matrix of the second fundamental form of the level surface

of ϕ at \mathbf{x} . One of the eigenvalues of Π is 0 which corresponds to the eigenvector $\nabla\phi$ and the other two eigenvalues of Π are the principal curvatures κ_1 and κ_2 of the level surface of ϕ at \mathbf{x} . The mean curvature H and Gaussian curvature K of the level surface are given, respectively, by

$$H = \frac{1}{2} \text{Trace}(\Pi), \quad (2.7)$$

$$K = \frac{1}{2} [(\text{Trace} \Pi)^2 - \text{Trace}(\Pi^2)]. \quad (2.8)$$

For convenience, we write $P = P(\phi)$, $\Pi = \Pi(\phi)$, $H = H(\phi)$, and $K = K(\phi)$, respectively, to indicate the dependence of these quantities on the level-set function ϕ . The following two useful identities are proved in Appendix:

$$\text{Trace}(\Pi(\phi)) = \frac{1}{|\nabla\phi|} P(\phi) : \nabla^2\phi; \quad (2.9)$$

$$\text{Trace}((\Pi(\phi))^2) = \frac{1}{|\nabla\phi|} \Pi(\phi) : \nabla^2\phi, \quad (2.10)$$

where $F : G = \sum_{i,j=1}^3 F_{ij} G_{ij}$ denotes the matrix product of two 3×3 matrices $F = (F_{ij})$ and $G = (G_{ij})$.

Notice that $A = A(\phi)$ in (2.2) defines a second-order nonlinear partial differential operator (applied to ϕ). We examine the parabolicity of the evolution equation

$$\phi_t = A(\phi) \quad (2.11)$$

at a given function ϕ . This is the parabolicity of the linearized equation at ϕ , namely,

$$\psi_t = \delta A(\phi)(\psi), \quad (2.12)$$

where $\delta A(\phi)$ is the Fréchet derivative of the operator A at ϕ . By a series of calculations presented in Appendix, we have

$$\delta A(\phi)(\psi) = \frac{d}{d\varepsilon} \Big|_{\varepsilon=0} A(\phi + \varepsilon\psi) = \gamma_0 D(\phi) : \nabla^2\psi + E(\nabla\phi, \nabla^2\phi, \nabla\psi), \quad (2.13)$$

where

$$D(\phi) = [1 - 4\tau H(\phi)P(\phi)] + 2\tau \Pi(\phi)$$

and the E term does not have any derivatives of ψ of order higher than one. The parabolicity of the linearized equation (2.12) is determined by the coefficients of the second derivatives of ψ , i.e., by the matrix $D(\phi)$. Note that the matrix $D(\phi)$ has the eigenvalues 0, $1 - 2\tau\kappa_1$, and $1 - 2\tau\kappa_2$. Therefore, Eq. (2.11) is degenerately parabolic at ϕ , or more precisely, parabolic in any direction tangential to the level surface of ϕ , if and only if

$$1 - 2\tau\kappa_1 > 0 \quad \text{and} \quad 1 - 2\tau\kappa_2 > 0. \quad (2.14)$$

We enforce the condition (2.14) when we discretize $A(\phi)$. By the definition of A (cf. (2.2)), (2.9), (2.10), and (2.7), we obtain

$$\begin{aligned}\frac{A(\phi)}{\gamma_0} &= 2[H(\phi) - \tau K(\phi)]|\nabla\phi| \\ &= \text{Trace}(\Pi(\phi))|\nabla\phi| - \tau[\text{Trace}(\Pi(\phi))]^2|\nabla\phi| + \tau\text{Trace}((\Pi(\phi))^2)|\nabla\phi| \\ &= P(\phi) : \nabla^2\phi - 2\tau H(\phi)(\Pi(\phi) : \nabla^2\phi) + \tau\Pi(\phi) : \nabla^2\phi.\end{aligned}$$

Therefore,

$$A(\phi) = \gamma_0 C(\phi) : \nabla^2\phi, \quad (2.15)$$

where the matrix $C(\phi)$ is given by

$$C(\phi) = [1 - 2\tau H(\phi)]P(\phi) + \tau\Pi(\phi). \quad (2.16)$$

Clearly, the matrix $C(\phi)$ is symmetric and has the eigenvalues 0, $1 - \tau\kappa_1$, and $1 - \tau\kappa_2$.

We use (2.15) to discretize the A part and to enforce the parabolicity. Since the equation $\phi_t = A(\phi)$ is of parabolic type after the parameter correction, we use the central differencing to discretize all the first-order and second-order derivatives of the level-set function ϕ at all the grid points, or those grid points in a narrow band around the surface Γ . (See more details in Step 2 of our algorithm described in the next section.) We then compute $H(\phi)$ by (2.7) and $C(\phi)$ by (2.16) at all the grid points in the band. We finally diagonalize the matrix $C(\phi)$ at such a grid point \mathbf{x} as

$$C(\phi) = Q^{-1} \begin{bmatrix} a_1 & 0 & 0 \\ 0 & a_2 & 0 \\ 0 & 0 & 0 \end{bmatrix} Q \quad (2.17)$$

for some real numbers $a_1 = a_1(\mathbf{x})$ and $a_2 = a_2(\mathbf{x})$, and an orthonormal matrix $Q = Q(\mathbf{x})$. The columns of Q consists of the unit vector along $\nabla\phi$ and its orthogonal vectors, all of which do not depend on τ . These numbers a_1 and a_2 are the eigenvalues $1 - \tau\kappa_1$ and $1 - \tau\kappa_2$ of $C(\phi)$ at \mathbf{x} .

The parabolicity condition (2.14) is equivalent to the following condition

$$1 - \tau\kappa_1 > 0.5 \quad \text{and} \quad 1 - \tau\kappa_2 > 0.5.$$

This is further equivalent to that $a_1 > 1/2$ and $a_2 > 1/2$. Therefore, we use the following correction to enforce the parabolicity condition:

$$\text{For } i = 1, 2: \quad \text{if } a_i < 0.5 \quad \text{then re-set } a_i = 0.5. \quad (2.18)$$

The new values a_1 and a_2 are put back into (2.17) which together with (2.15) are used as the $A(\phi)$ value at the point \mathbf{x} in the time iteration (cf. (2.19) below).

We now consider the discretization of the time derivative in the level-set equation (1.4) by an explicit scheme with a time stepping satisfying a CFL condition. Since we use the central

differencing to discretize the spatial derivatives of ϕ , which is of second-order accurate in space, and since the CFL condition for a second-order parabolic equation is $\Delta t = O(h^2)$, where Δt and h are the time and space step sizes, respectively, there is no need to use a high-order scheme, such as a high-order Runge-Kutta scheme, to discretize the time derivative. Therefore, we use the forward Euler method to discretize the time derivative in the level-set equation (1.4):

$$\frac{\phi^{(k+1)}(\mathbf{x}) - \phi^{(k)}(\mathbf{x})}{\Delta t_k} = -v_n^{(k)}(\mathbf{x}) |\nabla \phi^{(k)}(\mathbf{x})|, \quad (2.19)$$

where $\phi^{(k)}(\mathbf{x})$ and $v_n^{(k)}(\mathbf{x})$ are the approximations of $v_n(\mathbf{x}, t_k)$ and $\phi(\mathbf{x}, t_k)$, respectively, at time $t_k = t_{k-1} + \Delta t_{k-1}$ ($k = 1, 2, \dots$). As our analysis shows that our level-set equation consists of both second-order parabolic-like term A and first-order hyperbolic term $B|\nabla\phi|$ (cf. (2.1)), the corresponding CFL conditions are therefore $\Delta t = O(h^2)$ and $\Delta t = O(h)$, respectively. Hence, by interpolation, we choose

$$\Delta t = \frac{0.5h}{\max_{\mathbf{x}} [\text{Trace}(C(\mathbf{x}))/h + P + 2\rho_0|U(\mathbf{x})|]}, \quad (2.20)$$

where $C(\mathbf{x}) = C(\phi(\mathbf{x}))$ is defined in (2.16) but with the correction (cf. (2.17) and (2.18)), and the maximum is taken over all the grid points \mathbf{x} in the narrow band around the surface Γ in our local level-set method. Note that, after the parameter correction, the value $\text{Trace}(C(\mathbf{x}))$ is always positive. Note also that the time step size varies in the iteration.

3 Algorithm with Computational Details

Step 1. Input all the parameters P , γ_0 , τ , ρ_0 , ϵ_i and σ_i ($i = 1, \dots, N$), and the coordinates of all the points $\mathbf{x}_1, \dots, \mathbf{x}_N$.

Fix a computational box that contains all the points $\mathbf{x}_1, \dots, \mathbf{x}_N$ and discretize it with a uniform spatial grid size h . We usually choose h to be a third or half of one Angstrom, since all σ_i ($i = 1, \dots, N$) are around 2.5 to 4 Angstroms in applications. (We recall that each Lennard-Jones potential $U^{(i)}(r)$ defined in (1.3) reaches its minimum value at some point close to σ_i .) The size of the box is determined by the numerical resolution and the size of the narrow band around the surface in the local level-set method. Usually, the distance from a point \mathbf{x}_i ($1 \leq i \leq N$) to the surface Γ is in between σ_i and $3\sigma_i$. We choose the width of the narrow band to be 12 to 16 grid points, meaning that the distance between the surface and the boundary of the band is about 6 to 8 grid points. Therefore, we choose the computational box so that each point \mathbf{x}_i ($1 \leq i \leq N$) is about 15 grid points away from the boundary of the computational box.

Compute the function values P and $\rho_0 U(\mathbf{x})$ at all the grid points \mathbf{x} that are not any points $\mathbf{x}_1, \dots, \mathbf{x}_N$.

Generate an initial surface by defining a corresponding level-set function. We choose a level-set function to be negative inside and positive outside. Different initial surfaces

often lead to quite different final, steady-state surfaces that are local minima of the free-energy functional (1.1). To distinguish two classes of local minima, the drying and wetting structures that are of importance in molecular solvation, we have designed two classes of initial surfaces. One is a “tight wrap”, a surface that tightly wraps all the points $\mathbf{x}_1, \dots, \mathbf{x}_N$. The level-set function for such a surface is

$$\phi(\mathbf{x}) = \min_{1 \leq i \leq N} (|\mathbf{x} - \mathbf{x}_i| - \sigma_i).$$

The other is a “loose wrap”, a surface that loosely contains all the points $\mathbf{x}_1, \dots, \mathbf{x}_N$. An example of such a surface is a large sphere containing all these points.

Set $k = 1$ and start the time iteration.

Step 2. Choose a narrow band that is centered at the surface and that has the width about 12 to 16 grid points. We employ for efficiency the local level-set method developed in [16] in which the zero boundary condition is used for the level-set function ϕ at the boundary of the band.

At each grid point in the band, compute the gradient $\nabla\phi$, the Hessian $\nabla^2\phi$, and the mean curvature H . We use the central differencing to discretize all the first-order and second-order partial derivatives of ϕ at all the grid points inside the band. For grid points that are inside the band but close to the boundary of the band, we use lower-order finite-difference schemes to discretize those derivatives. This way, we reduce the influence of the homogeneous Dirichlet boundary conditions that we use on the boundary of the band. We use (2.7) to compute the mean curvature H .

Step 3. Compute the free energy (1.1). We use the following formulas to compute volume and surface integrals:

$$\begin{aligned} \int_{\Omega_{in}} f dV &= \int_{\mathbb{R}^3} (1 - Heav(\phi)) dV, \\ \int_{\Gamma} g dS &= \int_{\mathbb{R}^3} g |\nabla\phi| \delta(\phi) dV, \end{aligned}$$

where $Heav(\cdot)$ and $\delta(\cdot)$ are the Heaviside function and Dirac δ -function, respectively. We approximate the Dirac δ -function using the numerical δ -function proposed in [19] (cf. also [2]) which has the smallest support.

We have a special technique for the fast, accurate, and stable calculation of the integral of the Lennard-Jones potential. This technique is described in details in the next section.

Notice that it is not necessary to calculate the free energy in each time step. For instance, we can calculate the free energy for two consecutive steps after 50 or 100 steps. Differences of free-energy values corresponding to two consecutive steps are used to determine if the iteration should stop.

Step 4. Calculate and extend the normal velocity v_n using the decomposition (2.1). Continuing from Step 2, we compute the matrix $C(\phi)$ by (2.16) and diagonalize it as in (2.17). We then use (2.18) to modify $C(\phi)$ to enforce the parabolicity, and put the new $C(\phi)$ back to the A part using the formula (2.15).

For the B part in (2.1), we first use the level-set function, which has been kept close to a signed distance function (cf. Step 6 below), to locate by interpolation the points on the interface. We then calculate the values of the function $P - \rho_0 U$ at these points. We finally use a fast sweeping algorithm to extend these values in the normal direction (constant normal extension) to grid points in the narrow band of our local level-set method. Notice that the extended normal velocity in this part may not be the same as $P - \rho_0 U$. The reason that we do not use the default values of the function U away from the surface is that they change very rapidly near the surface, causing possibly numerical instabilities.

Step 5. Calculate Δt_k using (2.20) and update the level-set function using the Euler scheme (2.19). Before update, we use a fifth-order WENO method to discretize the part of the extension that corresponds to $P - \rho_0 U$.

Step 6. Reinitialize the level-set function ϕ . To do so, we solve the equation

$$\phi_t + \text{sign}(\phi_0)(|\nabla\phi| - 1) = 0 \quad (3.1)$$

with the initial value $\phi = \phi_0$ at $t = 0$ to obtain a steady-state solution. Here ϕ_0 is the level-set function before reinitialization, and the time t is different from that in the original level-set equation. The quantity $\text{sign}(\phi_0)$ is the sign of ϕ_0 and is approximated as

$$\text{sign}(\phi_0) = \frac{\phi_0}{\sqrt{\phi_0^2 + h}}$$

with h being the spatial step size [4]. For the sake of efficiency, Eq. (3.1) is solved with 12 iteration steps in time, using a fourth-order Runge-Kutta method in time and a fifth-order WENO scheme in space. We choose the time step size to be no bigger than $h/2$ to satisfy the CFL condition.

Step 7. Check for convergence by calculating the free energy (1.1). Stop if the free energy, or each part of the free energy, reaches a steady state. Otherwise locate the interface Γ by the level-set function obtained in the previous step, set $k := k + 1$, and go back to Step 2.

4 A Technique of Numerical Integration

Let us denote by Ω our computational box. To evaluate the free energy (1.1), we need to compute volume integrals of the Lennard-Jones potential. This amounts to computing

integrals of the form

$$I = \int_{\mathbb{R}^3 \setminus D} \frac{1}{|\mathbf{x} - \mathbf{x}_0|^k} dV,$$

where D is an open and bounded domain in \mathbb{R}^3 such that $D \subset \Omega$, $\mathbf{x}_0 \in D$, $k = 6$ or 12 (cf. (1.2) and (1.3)), and \mathbf{x} is the integral variable. To efficiently compute this integral, we break it into two integrals $I = I_1 + I_2$, where

$$I_1 = \int_{\Omega \setminus D} \frac{1}{|\mathbf{x} - \mathbf{x}_0|^k} dV \quad \text{and} \quad I_2 = \int_{\mathbb{R}^3 \setminus \Omega} \frac{1}{|\mathbf{x} - \mathbf{x}_0|^k} dV.$$

The first integral I_1 can be expressed by using the characteristic function $\chi_{\Omega \setminus D}$ as

$$I_1 = \int_{\Omega} \frac{\chi_{\Omega \setminus D}(\mathbf{x})}{|\mathbf{x} - \mathbf{x}_0|^k} dV.$$

This integral is over the computational box which is a cube. We approximate the characteristic function by a smooth function and then use the composite trapezoidal rule for each one-dimensional integral variable. The resulting numerical integration is still of second-order accurate.

To compute the second integral I_2 , we introduce the region

$$Q_1 = \left\{ (\rho, \varphi, \psi) : \frac{\alpha}{\cos \varphi \sin \psi} < \rho < \infty, \varphi_1 < \varphi < \varphi_2, 0 < \psi < \pi \right\}$$

in the local spherical coordinates centered at \mathbf{x}_0 with some real numbers α , φ_1 , and φ_2 . We also introduce the region

$$Q_2 = \left\{ (r, \theta, z) : 0 < r < \frac{\beta}{\cos \theta}, \theta_1 < \theta < \theta_2, L < z < \infty \right\}$$

in the local cylindrical coordinates centered at \mathbf{x}_0 with some real numbers β , θ_1 , θ_2 , and L . The region $\mathbb{R}^3 \setminus \Omega$ can be decomposed into several subregions, each of which is Q_1 or Q_2 with suitably chosen values of α , φ_1 , φ_2 , β , θ_1 , θ_2 , and L . Thus the integral I_2 is the sum of integrals of the following forms

$$I_{2,1} = \int_{Q_1} \frac{1}{|\mathbf{x} - \mathbf{x}_0|^k} dV = \int_0^\pi \int_{\varphi_1}^{\varphi_2} \int_{\frac{\alpha}{\cos \varphi \sin \psi}}^\infty \frac{\sin \psi}{\rho^{k-2}} d\rho d\theta d\psi$$

and

$$I_{2,2} = \int_{Q_2} \frac{1}{|\mathbf{x} - \mathbf{x}_0|^k} dV = \int_L^\infty \int_{\theta_1}^{\theta_2} \int_0^{\frac{\beta}{\cos \theta}} \frac{r}{(r^2 + z^2)^{k/2}} dr d\theta dz.$$

The integral $I_{2,1}$ can be calculated analytically. For the integral $I_{2,2}$, we can integrate analytically in the variable r and then in z , leaving finally a one-dimensional integral with respect to θ which can be computed numerically using the composite Simpson's rule.

We remark that computing the three-dimensional integration I_1 is the most costly step. In a case where D is changed but \mathbf{x}_0 is the same, the value of I_1 changes but that of I_2 remains the same.

5 Convergence Test

We test the accuracy and efficiency of our level-set method by applying it to a one-particle ($N = 1$) system. This system can be reformulated so that very accurate numerical solutions can be obtained by solving an optimization problem for a one-variable objective function. To see that, let us point out for this one-particle system that any possible solute-solvent interface is a sphere centered at \mathbf{x}_1 . We assume \mathbf{x}_1 is the origin and the radius of the sphere is $R > 0$. From (1.1), we obtain by some simple calculations the free energy now as a function of $R > 0$ (still use the notation G)

$$G(R) = \frac{4}{3}P\pi R^3 + 4\gamma_0\pi R^2 - 4\gamma_0\tau\pi R + 16\pi\rho_0\epsilon \left(\frac{\sigma^{12}}{9R^9} - \frac{\sigma^6}{3R^3} \right), \quad (5.1)$$

where $\sigma = \sigma_1$ and $\epsilon = \epsilon_1$. We use the following parameters that are close to real systems (cf. e.g., [3]): $P = 0$, $\gamma_0 = 0.15$, $\tau = 1.0$, $\rho_0 = 0.0333$, $\epsilon = 0.3$ and $\sigma = 3.5$. Here and below, we use $k_B T$ (with T around 300°K) and Angstrom (\AA) as the units of energy and length, respectively.

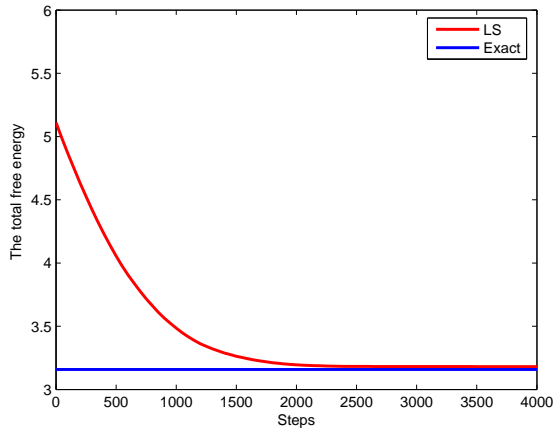


Figure 3: The decay of the free energy with respect to level-set iteration steps.

In Figure 3, we plot the free-energy values vs. the level-set iteration steps, where LS marks the level-set free-energy values and Exact means the exact minimum free energy. We see clearly that the free energy decays in the entire level-set relaxation process.

In Figure 4, we plot the minimum free energy of the one-particle system obtained using our level-set method (marked LS) and the spatial grid size h in the logarithmic scale. The convergence of the free-energy values to the exact value (marked Exact in Figure 4), which is obtained by minimizing the function $G(R)$ ($R > 0$) defined in (5.1), is clearly shown.

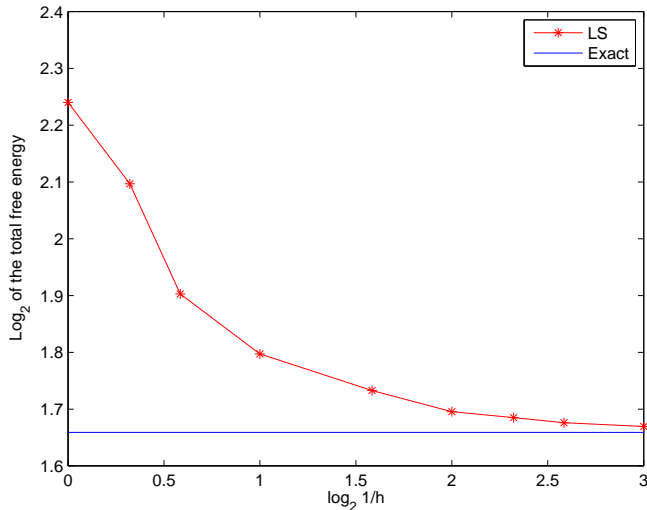


Figure 4: The free energy vs. step size in logarithmic scale.

6 Application to Molecular Solvation

6.1 A two-atom system

We place the centers of two particles at $\mathbf{x}_1 = (-d/2, 0, 0)$ and $\mathbf{x}_2 = (d/2, 0, 0)$, respectively, in the usual xyz coordinate system for some $d > 0$. The parameter d which is the center-to-center distance of the two particles is fixed for each of the level-set calculations. Our parameters are: $P = 0$, $\gamma_0 = 0.15$, $\tau = 1.0$, $\rho_0 = 0.0333$, $\epsilon_1 = \epsilon_2 = 0.3$, and $\sigma_1 = \sigma_2 = 3.5$. We set our initial surface to be either a “tight wrap” or a “loose wrap”. Both of them lead to the same final, (locally) free-energy minimizing surface. Figure 5 shows the cross section of such a free-energy minimizing surface at various distances. Notice that the surface has two components if the center-to-center distance is large.

6.2 A two-plate system

We consider two parallel plates of particles. Each plate has 11×11 particles. We use parameters similar to those in the previous example. In Figure 6, we plot cross sections of two types of initial surfaces, the tight wrap and the loose wrap, and their corresponding final surfaces obtained by our level-set computations for two separation distances d between the two plates. We see clearly that the tight and loose initials will result in different final minimum surfaces at separation distances d under consideration. (For large or small d , the tight and loose initial surfaces will lead to the same final surface.) This indicates that the free-energy functional (1.1) has usually many different local minima.

In terms of molecular modeling, the final surfaces displayed in Figure 6 corresponding to the loose initials (the second one and the fourth one in the right column) show the dewetting

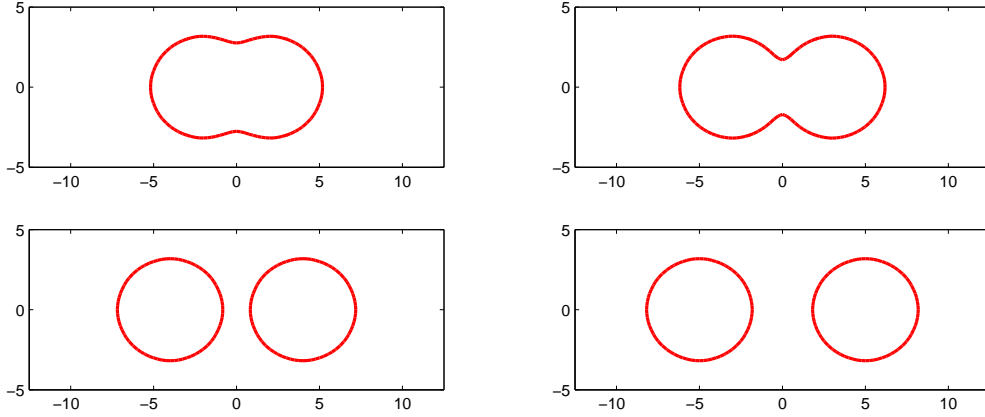


Figure 5: The cross section of the free-energy minimizing surface for the two-atom system at distance $d = 4\text{\AA}$ (upper left), $d = 6\text{\AA}$ (upper right), $d = 8\text{\AA}$ (lower left), and $d = 10\text{\AA}$ (lower right).

phenomenon, i.e., the solvent is excluded (even there is space for solvent molecules). This phenomenon is of importance in biological systems. Clearly, our underlying continuum solvent model and level-set method can capture such a phenomenon.

In Figure 7, we plot the free energy vs. the separation distance d for two cases. One is with a loose initial surface, a one-component surface that encloses all the atoms in the two plates. This loose surface leads to the final surface which describes the wetting of the system for a certain range of plate separations. The other one is with a tight initial surface, a two-component surface separating the two plates. We see clearly a hysteresis loop, indicating there is a transition between a wet state and a dry state.

6.3 A five-atom system

We consider an artificial system of 5 atoms located at $(0, 0, 0)$, $(-2, 0, 0)$, $(0, 2, 0)$, $(0, -2, 0)$, and $(a, 0, 0)$, where a is a parameter. We choose different values of a in between 2 and 9 to study the topological changes of the surface. We choose the parameters in the functional (1.1) same as before: $P = 0$, $\gamma_0 = 0.15$, $\tau = 1.0$, $\rho_0 = 0.0333$, all $\epsilon_i = 0.3$, and all $\sigma_i = 3.5$. Our level-set computational results are displaced in Figure 8 from which we see clearly the break of one component into two of the surface, as the distance between the fifth atom and the group of the first four atoms is large enough. The initial surface corresponding to the two-component final surface in the last case is a one-component “loose wrap”, a large surface enclosing all the 5 atoms. Our method captures the break-up of the surface during the relaxation.

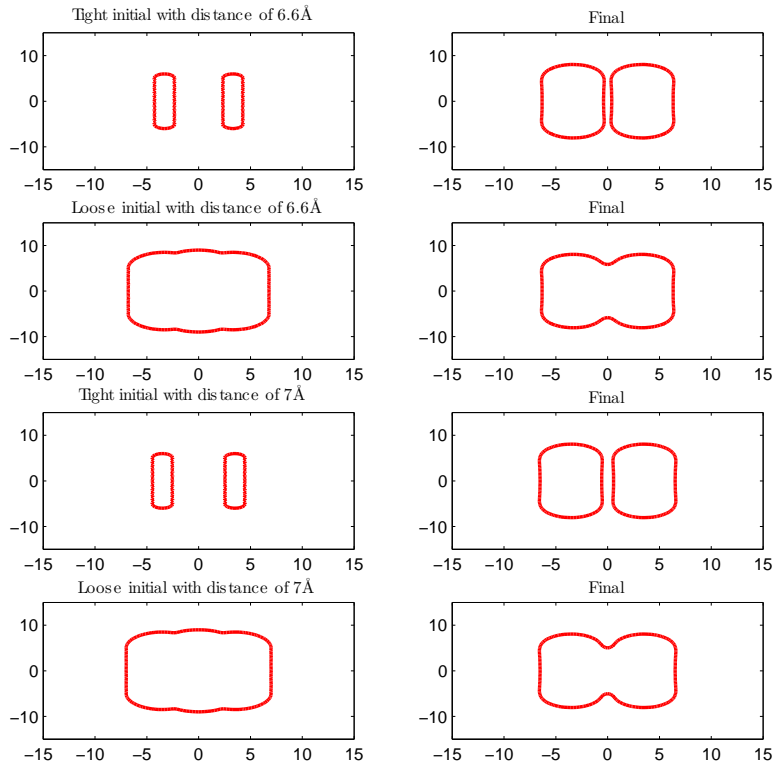


Figure 6: Cross sections of initial and final surfaces for the two-plate system at two different separations $d = 6.6 \text{ \AA}$ (left column) and $d = 7 \text{ \AA}$ (right column).

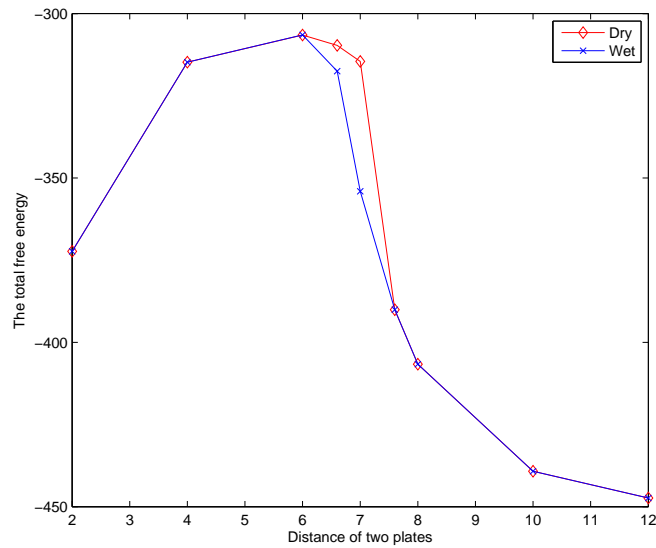


Figure 7: The free energy vs. the plate separation distance, showing a hysteresis loop.

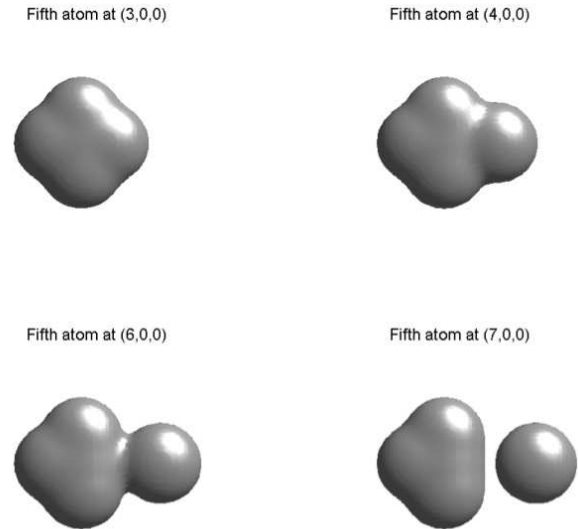


Figure 8: Topological changes in a system of 5 atoms.

6.4 A helical polymer

We consider a helical polymer of 32 atoms. Figure 9 shows some tight and loose initial surfaces and their corresponding final surfaces obtained by our level-set method. In this case, the final surfaces are the same.

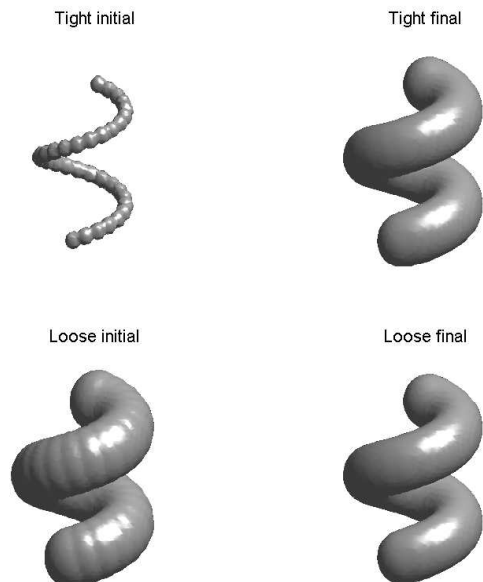


Figure 9: Two different initial surfaces and their corresponding final surfaces of a helical polymer.

6.5 An artificial molecule

We finally apply our level-set method to an artificial molecule that has about 800 atoms. Figure 10 shows the final, free-energy minimizing surface obtained by our level-set method. This example indicates that our method is capable of treating relatively large molecules.

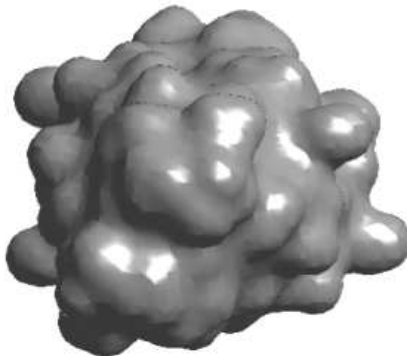


Figure 10: The free-energy minimizing surface of an artificial molecule calculated by the level-set method.

7 Conclusions

We have developed a level-set method for numerically capturing stable, free-energy minimizing, solute-solvent interfaces for complex shaped molecules in three-dimensional space. The free-energy functional, defined on possible surfaces that enclose fixed points representing atoms of solute molecules, has the main terms of the Hadwiger valuations and a lower-order term that models the interaction between solute atoms and the solvent molecules that are coarse-grained.

Our level-set method solves a geometrical problem of surface motion whose normal velocity is a linear combination of the mean curvature, the Gaussian curvature, and a lower-order forcing term. The key feature in our method is the enforcement of parabolicity based on our linear analysis of the stability of the underlying surface motion. We apply and improve many of the state-of-the-art level-set techniques that include the local level-set method, a high-accurate upwinding discretization, and the reinitialization of the level-set function. We also develop an accurate, fast, and stable technique for the numerical integration of the Lennard-Jones potential which is a source of instability due to its rapid change of values. Numerical tests and applications demonstrate that our method is robust in terms of the accuracy and efficiency.

Currently, we are working to extend our models and methods in several aspects.

- (1) Add the surface integral of the Gaussian curvature to the free-energy function (1.1). While the physical meaning of the coefficient of this term is not quite clear to us, it

is challenging mathematically and numerically to design a level-set technique to treat this new term.

- (2) Include the electrostatic free energy in our free-energy functional (1.1). This requires, in the continuum modeling, solutions of a partial differential equation to get the electrostatic potential for calculating the electrostatic free energy. There has been much in the literature on this issue. We shall revisit it in the context of the level-set method.
- (3) From our numerical simulations, we observe the cancellation of large numbers in magnitude of the geometrical part (e.g., the surface area) and the Lennard-Jones part of the total free energy. This cancellation results in the loss of accuracy if not properly handled. A further study on this numerical issue is necessary.
- (4) Increasing the efficiency is a very challenging issue, and we are working on this using different kinds of fast numerical methods.

Acknowledgments

This work was supported by the US National Science Foundation (NSF) through grant DMS-0811259 (B. L.), by the Center for Theoretical Biological Physics (CTBP) through the NSF grant PHY-0822283 (B. L. and Z. W.), and by the US Department of Energy through grant DE-FG02-05ER25707 (B. L.). Z. W. was supported by Professor J. Andrew McCammon's research grant. The authors thank Dr. Jianwei Che, Dr. Joachim Dzubiella, Dr. Piotr Setny, and Professor J. Andrew McCammon for helpful discussions. The authors also thank Dr. Jianwei Che for providing the data of the artificial molecule we used in the last subsection of Section 6.

Appendix

We first prove (2.9) and (2.10). By the definition of $P = P(\phi) = (P_{ij})$ and $\Pi = \Pi(\phi)$ (cf. (2.5)), and the fact that $P^2 = P$, we have

$$\begin{aligned}
 \text{Trace}(\Pi(\phi)) &= \frac{1}{|\nabla\phi|} \sum_{i,k,l=1}^3 P_{ik} (\partial_{kl}^2\phi) P_{li} \\
 &= \frac{1}{|\nabla\phi|} \sum_{k,l=1}^3 \left(\sum_{i=1}^3 P_{li} P_{ik} \right) \partial_{kl}^2\phi \\
 &= \frac{1}{|\nabla\phi|} \sum_{k,l=1}^3 P_{lk} \partial_{lk}^2\phi
 \end{aligned}$$

$$= \frac{1}{|\nabla\phi|} P(\phi) : \nabla^2\phi.$$

This proves (2.9). Similarly, we obtain also by the symmetry of the matrix P that

$$\begin{aligned} \text{Trace}((\Pi(\phi))^2) &= \frac{1}{|\nabla\phi|^2} \text{Trace}(P(\nabla^2\phi)P(\nabla^2\phi)P) \\ &= \frac{1}{|\nabla\phi|^2} \sum_{i,k,l,r,s=1}^3 P_{ik}(\partial_{kl}^2\phi)P_{lr}(\partial_{rs}^2\phi)P_{si} \\ &= \frac{1}{|\nabla\phi|^2} \sum_{k,l,r,s=1}^3 P_{sk}(\partial_{kl}^2\phi)P_{lr}(\partial_{rs}^2\phi) \\ &= \frac{1}{|\nabla\phi|} \Pi(\phi) : \nabla^2\phi, \end{aligned}$$

proving (2.10).

We now derive (2.13). Using the definition of P (cf. (2.5)) and the Taylor expansion, we obtain after some elementary calculations that

$$\begin{aligned} P(\phi + \varepsilon\psi) &= I - \frac{(\nabla\phi + \varepsilon\nabla\psi) \otimes (\nabla\phi + \varepsilon\nabla\psi)}{|\nabla\phi + \varepsilon\nabla\psi|^2} \\ &= P(\phi) + \varepsilon P_1 + O(\varepsilon^2) \end{aligned} \tag{A.1}$$

for small $\varepsilon > 0$, where

$$P_1 = \frac{2(\nabla\phi \cdot \nabla\psi)}{|\nabla\phi|^4} \nabla\phi \otimes \nabla\psi - \frac{1}{|\nabla\phi|^2} (\nabla\phi \otimes \nabla\psi + \nabla\psi \otimes \nabla\phi).$$

Similarly, we have by (2.6) and (A.1) that

$$\begin{aligned} \Pi(\phi + \varepsilon\psi) &= \frac{1}{|\nabla\phi + \varepsilon\nabla\psi|} P(\nabla\phi + \varepsilon\nabla\psi)(\nabla^2\phi + \varepsilon\nabla^2\psi)P(\nabla\phi + \varepsilon\nabla\psi) \\ &= \frac{1}{|\nabla\phi|(1 + 2\varepsilon\nabla\phi \cdot \nabla\psi)^{1/2}} (P_0 + \varepsilon P_1)(\nabla^2\phi + \varepsilon\nabla^2\psi)(P_0 + \varepsilon P_1) + O(\varepsilon^2) \\ &= \Pi(\phi) + \varepsilon\Pi_1 + O(\varepsilon^2), \end{aligned} \tag{A.2}$$

where

$$\begin{aligned} \Pi_1 &= \frac{1}{|\nabla\phi|} \left[P(\phi)(\nabla^2\phi)P_1 + P_1(\nabla^2\phi)P(\phi) - \frac{(\nabla\phi \cdot \nabla\psi)}{|\nabla\phi|^3} P(\phi)(\nabla^2\phi)P(\phi) + P(\phi)(\nabla^2\psi)P(\phi) \right] \\ &= \frac{1}{|\nabla\phi|} P(\phi)(\nabla^2\psi)P(\phi) + F(\nabla\phi, \nabla^2\phi, \nabla\psi), \end{aligned} \tag{A.3}$$

where the F term does not have any of the second derivatives of ψ .

By (2.7) and (2.9), we have

$$2H(\phi)|\nabla\phi| = P(\phi) : \nabla^2\phi.$$

This and (A.1) lead to

$$\begin{aligned} 2H(\phi + \varepsilon\psi)|\nabla\phi + \varepsilon\nabla\psi| &= P(\phi + \varepsilon\psi) : (\nabla^2\phi + \varepsilon\nabla^2\psi) \\ &= 2H(\phi)|\nabla\phi| + \varepsilon [P_1 : \nabla^2\phi + P(\phi) : \nabla^2\psi] + O(\varepsilon^2). \end{aligned} \quad (\text{A.4})$$

By (2.8), (2.7), (2.9), and (2.10), we obtain

$$\begin{aligned} 2K(\phi)|\nabla\phi| &= |\nabla\phi| [(\text{Trace } \Pi(\phi))^2 - \text{Trace } ((\Pi(\phi))^2)] \\ &= \frac{1}{|\nabla\phi|} [P(\phi) : \nabla^2\phi]^2 - \Pi(\phi) : \nabla^2\phi. \end{aligned}$$

This, together with (A.1), (A.2), (A.3), (2.9), and (2.7), implies that

$$\begin{aligned} &2K(\phi + \varepsilon\psi)|\nabla\phi + \varepsilon\nabla\psi| \\ &= \frac{1}{|\nabla\phi + \varepsilon\nabla\psi|} [P(\phi + \varepsilon\psi) : (\nabla^2\phi + \varepsilon\nabla^2\psi)]^2 - \Pi(\phi + \varepsilon\psi) : (\nabla^2\phi + \varepsilon\nabla^2\psi) \\ &= \left[\frac{1}{|\nabla\phi|} - \varepsilon \frac{\nabla\phi \cdot \nabla\psi}{|\nabla\phi|^3} \right] \{ [P(\phi) + \varepsilon P_1] : (\nabla^2\phi + \varepsilon\nabla^2\psi) \}^2 \\ &\quad - [\Pi(\phi) + \varepsilon\Pi_1] : (\nabla^2\phi + \varepsilon\nabla^2\psi) + O(\varepsilon^2) \\ &= \left[\frac{1}{|\nabla\phi|} - \varepsilon \frac{\nabla\phi \cdot \nabla\psi}{|\nabla\phi|^3} \right] [P(\phi) : \nabla^2\phi + \varepsilon P_1 : \nabla^2\phi + \varepsilon P(\phi) : \nabla^2\psi]^2 \\ &\quad - \Pi(\phi) : \nabla^2\phi - \varepsilon\Pi_1 : \nabla^2\phi - \varepsilon\Pi(\phi) : \nabla^2\psi + O(\varepsilon^2) \\ &= \frac{1}{|\nabla\phi|} [P(\phi) : \nabla^2\phi]^2 - \Pi(\phi) : \nabla^2\phi \\ &\quad + \varepsilon \left\{ \frac{2[P(\phi) : \nabla^2\phi][P(\phi) : \nabla^2\psi]}{|\nabla\phi|} - \frac{P(\phi)(\nabla^2\psi)P(\phi) : \nabla^2\phi}{|\nabla\phi|} - \Pi(\phi) : \nabla^2\psi \right\} \\ &\quad + \varepsilon G(\nabla\phi, \nabla^2\phi, \nabla\psi) + O(\varepsilon^2) \\ &= 2K(\phi)|\nabla\phi| + \varepsilon \left[4H(\phi)P(\phi) : \nabla^2\psi - \frac{P(\phi)(\nabla^2\psi)P(\phi) : \nabla^2\phi}{|\nabla\phi|} - \Pi(\phi) : \nabla^2\psi \right] \\ &\quad + \varepsilon G(\nabla\phi, \nabla^2\phi, \nabla\psi) + O(\varepsilon^2), \end{aligned} \quad (\text{A.5})$$

where the G term does not depend on any of the second derivatives of ψ . By (2.9) and the symmetry of a Hessian matrix, we obtain that

$$\begin{aligned} \frac{P(\phi)(\nabla^2\psi)P(\phi) : \nabla^2\phi}{|\nabla\phi|} &= \frac{1}{|\nabla\phi|} \text{Trace } (P(\phi)(\nabla^2\psi)P(\phi)(\nabla^2\phi)) \\ &= \frac{1}{|\nabla\phi|} \text{Trace } (P(\phi)(\nabla^2\phi)P(\phi)(\nabla^2\psi)) \end{aligned}$$

$$\begin{aligned}
&= \frac{1}{|\nabla\phi|} [P(\phi)(\nabla^2\phi)P(\phi) : \nabla^2\psi] \\
&= \Pi(\phi) : \nabla^2\psi.
\end{aligned}$$

This and (A.5) imply that

$$\begin{aligned}
2K(\phi + \varepsilon\psi)|\nabla\phi + \varepsilon\nabla\psi| &= 2K(\phi)|\nabla\phi| + \varepsilon [4H(\phi)P(\phi) : \nabla^2\psi - 2\Pi(\phi) : \nabla^2\psi] \\
&\quad + \varepsilon G(\nabla\phi, \nabla^2\phi, \nabla\psi) + O(\varepsilon^2).
\end{aligned} \tag{A.6}$$

Now the desired result (2.13) follows from (A.4) and (A.6).

References

- [1] L. Ambrosio and H. M. Soner. Level set approach to mean curvature flow in arbitrary codimension. *J. Diff. Geom.*, 43:693–737, 1996.
- [2] J. T. Beale. A proof that a discrete delta function is second-order accurate. *J. Comput. Phys.*, 227:2195–2197, 2008.
- [3] L.-T. Cheng, J. Dzubiella, J. A. McCammon, and B. Li. Application of the level-set method to the implicit solvation of nonpolar molecules. *J. Chem. Phys.*, 127:084503, 2007.
- [4] L.-T. Cheng and Y.-H. Tsai. Redistancing by flow of time dependent eikonal equation. *J. Comput. Phys.*, 227:4002–4017, 2008.
- [5] L.-T. Cheng, Z. Wang, P. Setny, J. Dzubiella, B. Li, and J. A. McCammon. Interfaces and hydrophobic interactions in receptor-ligand systems: A level-set variational implicit solvent approach. *J. Chem. Phys.*, 131:144102, 2009.
- [6] L.-T. Cheng, Y. Xie, J. Dzubiella, J. A. McCammon, J. Che, and B. Li. Coupling the level-set method with molecular mechanics for variational implicit solvation of nonpolar molecules. *J. Chem. Theory Comput.*, 5:257–266, 2009.
- [7] J. Dzubiella, J. M. J. Swanson, and J. A. McCammon. Coupling hydrophobicity, dispersion, and electrostatics in continuum solvent models. *Phys. Rev. Lett.*, 96(8):087802, 2006.
- [8] J. Dzubiella, J. M. J. Swanson, and J. A. McCammon. Coupling nonpolar and polar solvation free energies in implicit solvent models. *J. Chem. Phys.*, 124:084905, 2006.
- [9] L. C. Evans and J. Spruck. Motion of level sets by mean curvature. *J. Diff. Geom.*, 33:635–681, 1991.
- [10] H. Hadwiger. *Vorlesungen über Inhalt, Oberfläche und Isoperimetrie*. Springer-Verlag, Berlin, 1957.

- [11] D. A. Klain and G.-C. Rota. *Introduction to geometric probability*. Cambridge University Press, Cambridge, 1997.
- [12] S. Osher and R. Fedkiw. *Level Set Methods and Dynamic Implicit Surfaces*, volume 153 of *Applied Mathematical Sciences*. Springer-Verlag, 2003.
- [13] S. Osher and J. A. Sethian. Fronts propagating with curvature-dependent speed: Algorithms based on Hamilton-Jacobi formulations. *J. Comput. Phys.*, 79(1):12–49, 1988.
- [14] Z. Ou-Yang and W. Helfrich. Bending energy of vesicle membranes: General expressions for the first, second, and third variation of the shape energy and applications to spheres and cylinders. *Phys. Rev. A*, 39(10):5280–5288, 1989.
- [15] N. C. Overgaard and J. E. Solem. The variational origin of motion by Gaussian curvature. In *Scale Space and Variational Methods in Computer Vision*, volume 4485 of *Lecture Notes in Computer Science*, pages 430–441. Springer, 2007.
- [16] D. Peng, B. Merriman, S. Osher, H. Zhao, and M. Kang. A PDE-based fast local level set method. *J. Comput. Phys.*, 155(2):410–438, 1999.
- [17] James A. Sethian. *Level Set Methods and Fast Marching Methods : Evolving Interfaces in Computational Geometry, Fluid Mechanics, Computer Vision, and Materials Science*. Cambridge, 1999.
- [18] P. Setny, Z. Wang, L.-T. Cheng, B. Li, J. A. McCammon, and J. Dzubiella. Dewetting-controlled binding of ligands to hydrophobic pockets. *Phys. Rev. Lett.*, 103:187801, 2009.
- [19] P. Smereka. The numerical approximation of a delta function with application to level set methods. *J. Comput. Phys.*, 211(1):77–90, 2006.